

THE EXTENDED GAIA-PS1-SDSS (GPS1+) PROPER MOTION CATALOG

HAI-JUN TIAN^{1,2}, YANG XU³, CHAO LIU³, HANS-WALTER RIX², BRANIMIR SESAR² BERTRAND GOLDMAN^{2,4}

Draft version February 5, 2022

ABSTRACT

The GPS1 catalog was released in 2017. It delivered precise proper motions for around 350 million sources across three-fourths of the sky down to a magnitude of $r \sim 20$ mag. In this study, we present GPS1+ the extension GPS1 catalog down to $r \sim 22.5$ mag, based on *Gaia* DR2, PS1, SDSS and 2MASS astrometry. The GPS1+ totally provides proper motions for ~ 400 million sources with a characteristic systematic error of less than 0.1 mas yr^{-1} . This catalog is divided into two sub-samples, i.e., the primary and secondary parts. The primary ~ 264 million sources have either or both of the *Gaia* and SDSS astrometry, with a typical precision of $2.0\text{--}5.0 \text{ mas yr}^{-1}$. In this part, ~ 160 million sources have *Gaia* proper motions, we provide another new proper motion for each of them by building a Bayesian model. Relative to *Gaia*'s values, the precision is improved by ~ 0.1 dex on average at the faint end; ~ 50 million sources are the objects whose proper motions are missing in *Gaia* DR2, we provide their proper motion with a precision of $\sim 4.5 \text{ mas yr}^{-1}$; the remaining ~ 54 million faint sources are beyond *Gaia* detecting capability, we provide their proper motions for the first time with a precision of 7.0 mas yr^{-1} . However, the secondary ~ 136 million sources only have PS1 astrometry, the average precision is worse than 15.0 mas yr^{-1} . All the proper motions have been validated using QSOs and the existing *Gaia* proper motions. The catalog will be released on-line and available via the TAP Service, or via the National Astronomical Data Center serviced by China-VO: <https://nadc.china-vo.org/data/data/gps1p/f>

Keywords: astrometry - catalogs - Galaxy: kinematics and dynamics - proper motions

1. INTRODUCTION

Gaia, a cornerstone mission of the European Space Agency (ESA), is ambitious to chart a three-dimensional map of our Galaxy with unprecedented precision. After 22 months of observations, *Gaia* delivered its second release (*Gaia* DR2) on April 25, 2018 (*Gaia* Collaboration et al. 2018). This catalog contains the positions of nearly 1.7 billion objects with G -band magnitude brighter than ~ 20.7 . Among these sources, more than 1.3 billion stars in the Milk Way have precise positions, proper motions, parallaxes and colors. The average uncertainties in the respective proper motion components are up to 0.06 mas yr^{-1} (for $G < 15$ mag), 0.2 mas yr^{-1} (for $G = 17$ mag) and 1.2 mas yr^{-1} (for $G = 20$ mag). The *Gaia* DR2 parallaxes and proper motions are based only on *Gaia* data.

The *Gaia* DR2 supersedes the most majority of current existing proper motion catalogs. The previous proper motion catalogs, such as PPMXL (Roeser et al. 2010), HSOY (Altmann et al. 2017), the UCAC series (Zacharias et al. 2004, 2010; Zacharias et al. 2017), APOP (Qi et al. 2015), and GPS1 (Tian et al. 2017a, hereafter, T17), are not comparable with *Gaia* DR2 in quality, even though HSOY, UCAC5 and GPS1 were built combining the precise *Gaia* DR1 astrometry (*Gaia* Collaboration et al. 2016).

Unfortunately, some limitations still exists in *Gaia* DR2: (1) more than 361 million sources only have positions (precision ~ 2 mas) at J2015.5 and the mean G magnitude, missing proper motions and parallax etc; (2) the average precision of

proper motions is hard to reach a level of sub-mas yr^{-1} for faint sources, in particular for those close to the *Gaia* limiting magnitude; (3) *Gaia* DR2 is complete in $12 < G < 17$ mag, but incomplete at an ill-defined faint magnitude limit; (4) no sources with $G > 20.7$ mag.

In this study, we would like to extend the GPS1, and release GPS1+ proper motion catalog to make up the limitations of *Gaia* DR2. Therefore, the GPS1+ will mainly focus on: (1) the sources ($19 < G < 20.7$ mag), using the *Gaia* DR2 proper motions as priors to improve the proper motions combining PS1 and SDSS if their proper motions were measured in *Gaia* DR2; (2) the part of missing sources (> 361 million) in *Gaia* DR2, their proper motions are calculated with the same procedure of GPS1; (3) the faint sources ($20.7 < G < 22.5$ mag), using the same procedure as GPS1.

With the above motivations, we arrange the remainder of this paper as follows. In Section 2, we describe how to construct the GPS1+ catalog. In this section, we first summarize the four data sets in brief, and describe a Bayesian model to calculate proper motions for the sources which have *Gaia* proper motions. Section 3 then presents the results of GPS1+ proper motions, and demonstrate their performance in accuracy and precision. In Section 4, we briefly discuss the limitations of GPS1+ and summarize in Section 5.

Throughout the paper, we adopt the Solar motion as $(U_{\odot}, V_{\odot}, W_{\odot}) = (9.58, 10.52, 7.01) \text{ kms}^{-1}$ (Tian et al. 2015), and the IAU circular speed of the local standard of rest (LSR) as $v_0 = 220 \text{ kms}^{-1}$. Also, α^* is used to denote the right ascension in the gnomonic projection coordinate system, for example, $\mu_{\alpha^*} = \mu_{\alpha} \cos(\delta)$, and $\Delta\alpha^* = \Delta\alpha \cos(\delta)$, while ϵ denotes uncertainties, to avoid confusion with the symbol δ referring to a source's declination. We use Δ to denote the differences in quantities such as proper motion or position.

2. THE CONSTRUCTION OF GPS1+

2.1. Data Set

¹ Center for Astronomy and Space Sciences, China Three Gorges University, Yichang 443002, China.

² Max Planck Institute for Astronomy, Königstuhl 17, D-69117 Heidelberg, Germany. Email: hjtian@lamost.org

³ Key Lab for Optical Astronomy, National Astronomical Observatories, Chinese Academy of Sciences, Beijing 100012, China.

⁴ Observatoire astronomique de Strasbourg, Université de Strasbourg, CNRS, UMR 7550, 11 rue de l'Université, F-67000 Strasbourg, France.

We still use the four basic imaging surveys, i.e., *Gaia*, PS1, SDSS, and 2MASS, to build the GPS1+ catalog. Unlike GPS1, GPS1+ will be based on the *Gaia* DR2, but the other three astrometric datasets keep the same as those used in GPS1, i.e., the same data version and treatment.

Gaia DR2 consists of around 1.69 billion astrometric sources (*Gaia* Collaboration et al. 2018). All the sources have positions, and they are calibrated to the International Celestial Reference Frame (ICRF) at epoch J2015.5. The typical uncertainties in positions are the order of 0.7 mas for sources at the faint end (i.e., $G = 20$ mag), as shown in the top panel of Figure 1. Therefore, *Gaia* DR2 is able to provide one precise observational position at epoch J2015.5. The epoch is different from J2015.0 in *Gaia* DR1.

About 1.33 billion sources have proper motions, but more than 361 million sources have no proper motions in *Gaia* DR2. The sources missing proper motions are mainly located at the faint region in *Gaia* DR2, as shown in the top panel of Figure 2 by comparing the histograms between the entire sources (blue) and those without proper motions (green) in *Gaia* DR2. The bottom panel of Figure 2 displays the scatter distribution of the uncertainties of *Gaia* DR2 proper motions at the faint region ($r > 19$ mag). The red points are the median uncertainties of proper motions in different magnitude bins. The median uncertainty is larger than 2.0 mas yr^{-1} (marked with the black dashed line) for the sources close to the limiting magnitude. The proper motion precision of these sources will be significantly improved by combining the astrometry of PS1, SDSS and *Gaia*. This point will be demonstrated in Section 2.2.

Pan-STARRS1 (PS1; Chambers 2011) is a wide-field optical/near-IR survey telescope system, which has been conducting multi-epoch and multi-color observations over the entire sky visible from Hawaii (decl. $\gtrsim -30^\circ$) for many years. Its Processing Version 3 catalog (PV3; Chambers et al. 2016) contained around 65 detections for each source over a sky area of $\sim 30,000 \text{ deg}^2$ with epochs throughout the 5.5 years from 2010 to 2014.

As does in GPS1, we take season averages and positional uncertainties for the faint sources ($r_{\text{PS1}} > 19.0$ mag) in PS1. Each source is detected more than 10 times in an observing season. The typical single-epoch positional precision of faint sources is ~ 50 mas, as illustrated in the second panel of Figure 1. Furthermore, we apply the selection cuts used in GPS1 on the individual detections and the individual faint sources to remove the PS1 astrometry outliers. Finally, we obtain around 400 million faint objects with billions of detections.

The Sloan Digital Sky Survey (SDSS) began its regular operations in 2000 April (York et al. 2000). Its ninth data release (DR9) almost contains its all the photometric data (Ahn et al. 2012), which were imaged in the early epochs, e.g. 10–20 years ago. The long epoch baseline makes this data very valuable. The typical astrometric uncertainties for faint stars ($r > 19.0$ mag) are around 80 mas per coordinate (Stoughton et al. 2002), as shown in the third panel of Figure 1.

Two Micron All Sky Survey (2MASS; Skrutskie et al. 2006) All-Sky Data Release identifies around 471 million point sources, and 1.6 million extended sources, covering virtually the entire celestial sphere between June 1997 and February 2001. Faint source extractions have the astrometric accuracy of the order 100 mas, as shown in the bottom panel of Figure 1. Because of large positional uncertainties, 2MASS positions provide only a weak constraint for proper motion measurements.

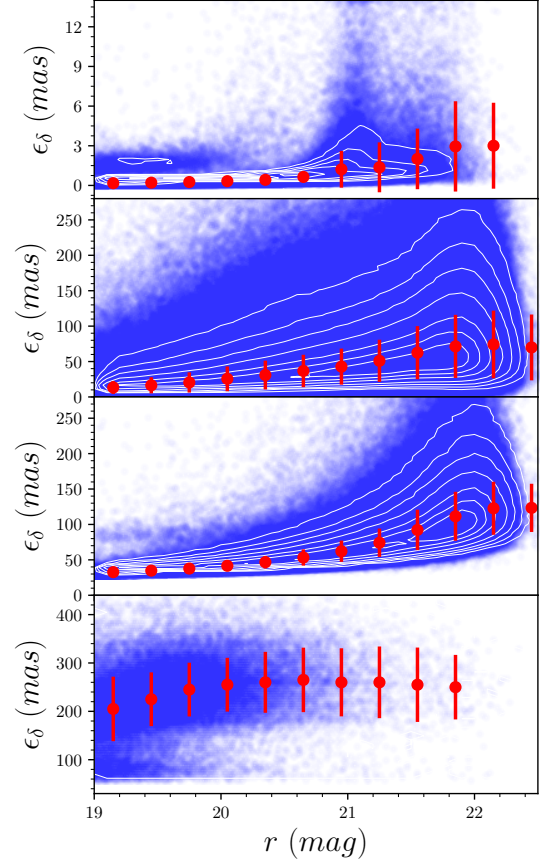


Figure 1. Precision of the source position measurements along the δ direction for the various data sets used in the construction of the GPS1+ catalog, as a function of r -band magnitude. The red dots and bars indicate the average and root-mean-square (rms) of the position uncertainties in each magnitude bin. The average position uncertainties are 0.5, 50, 80, and 235 mas for the entire samples in $19 < r < 22.5$ mag from *Gaia* DR2, PS1, SDSS, and 2MASS, respectively. The contours indicate the normalized number density of sources with different levels of 0.02, 0.05, 0.1, 0.2, 0.4, 0.6, and 0.8 (the highest density is normalized to 1).

We cross-matched the PS1 objects with *Gaia*, 2MASS and SDSS using a $1.5''$ search radius. Therefore, the internal ID from PS1 is the key identifier to connect the four catalogs.

The black histogram in Figure 2 indicates that there are more than 60% PS1 sources beyond *Gaia*’s limiting magnitude. These sources ($>70\%$) without *Gaia* (including *Gaia* missing) proper motions will be our main interest in this study.

2.2. Derivation of Proper Motions

Proper motions in GPS1+ are determined basically with the same procedure used in GPS1. The key difference just takes place on the sources which have *Gaia* proper motions. For these sources, we calculate two kinds of proper motions for each source: one is with the method of GPS1, i.e., by performing a linear least-squares fit; the other is fitted through a Bayesian model which uses *Gaia* proper motions as priors and combines the astrometry of *Gaia*, PS1, SDSS and 2MASS. It is worth to mention that both of the two fit methods do not involve *Gaia* parallax, so the derived proper motions will be away from the impact of parallax, unlike *Gaia*’s proper motions which is correlated with the parallax.

With the procedure of GPS1 construction, we build a reference catalog by averaging repeatedly observed positions of

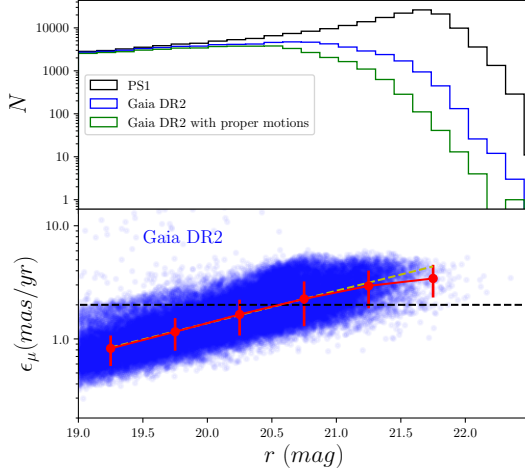


Figure 2. Top: the histograms of the sources at the faint region ($r > 19$ mag) from *Gaia* DR2 (blue), PS1 (black), and *Gaia* DR2 in which sources have proper motions (green), in the same sky region. The sources with *Gaia* proper motions only take fraction of $\sim 40\%$ in a sample selected from PS1 in a random sky region. Bottom: the uncertainties distribution of *Gaia* DR2 proper motions at the faint region ($r > 19$ mag). The uncertainties increase with magnitudes as a function of a power law, i.e., **the flux in r band to the 0.29 power** (the yellow dashed line). The average uncertainty of the proper motions is larger than 2 mas yr^{-1} (marked with the black dashed line) for the sources nearby the *Gaia* limiting magnitude.

PS1 galaxies in each tile (i.e., a sky area of a constant size of 10° by 10°), and calibrate the cataloged positions for each object in five (or six) PS1 epochs, one *Gaia* epoch, possibly one SDSS epoch and one 2MASS epoch onto the same reference frame. All the steps have been minutely summarized in Section 3 of T17. For each source, we calculate its proper motion by performing a linear least squares fit based on a simple χ^2 which is described in Equation (2) of T17. But for a source which has a *Gaia* proper motion, we re-measure another new proper motion by building a Bayesian model. We start with a likelihood

$$L = p(\{t_i, y_i\} | \mu, b) = \prod_i \left\{ \frac{1}{\sqrt{\epsilon_i^2}} \exp \left[-\frac{[\hat{y}_i^o - y_i^{\text{model}}(t_i)]^2}{2\epsilon_i^2} \right] \right\}, \quad (1)$$

where \hat{y}_i^o is the observed position of a star with a positional uncertainty ϵ_i at epoch i . The positional uncertainty ϵ_i consists of two parts: one part is the individual position precision, illustrated in Figure 1; and the other part is the uncertainty from the offset calibration discussed in Section 3.2 of T17. $y_i^{\text{model}}(t_i)$ is the predicted position by a linear model at the given time t_i , i.e., $y_i^{\text{model}}(t_i) = \mu t_i + b$, N is the number of epochs in different surveys. The position \hat{y}_i^o has been calibrated by

$$\hat{y}_i^o = y_i^o - \Delta_i(\alpha, \delta) - \Delta_i(\delta, m), \quad (2)$$

where y_i^o is the original cataloged position of a star at epoch i , $\Delta_i(\alpha, \delta)$ is the direction dependent offset described in Section 3.2.1 of T17, and $\Delta_i(\delta, m)$ is the magnitude and declination dependent offset described in Section 3.2.2 of T17.

According to Bayes theorem, the posterior probability can be easily expressed as

$$p(\{\mu, b | t_i, y_i\}) = p(\{t_i, y_i\} | \mu, b) p(\mu) p(b), \quad (3)$$

we assume the prior probability of μ obeys a Gaussian distribution with $\bar{\mu} = \mu_{\text{Gaia}}$ and $\sigma = \epsilon_{\text{Gaia}}$, where μ_{Gaia} and ϵ_{Gaia} are the proper motion and uncertainty values of a source provided by *Gaia* DR2. We assume a flat prior probability of b ,

i.e., $p(b) = 1$.

We use *emcee* (Foreman-Mackey et al. 2013) to sample the posterior distribution (Equation 3) and estimate proper motions in the two directions, i.e., μ_{α^*} and μ_{δ} , respectively. In practice, we could use the joint posterior probability to constrain μ_{α^*} and μ_{δ} , simultaneously. The intercept b is also a free parameter in the MCMC sampling, but its value is not important for this study. Figure 3 illustrates two examples of proper motion contours and marginalized probability distributions of two sources with different magnitudes. The *Gaia* detector takes on different performances for sources with distinct brightness. For instance, *Gaia* is able to measure a good position for a source with $r = 19.6$ mag. Thus, the combination of the multi-surveys can not significantly improve the precision of the *Gaia* proper motion (only by $\Delta\epsilon_\mu \sim 0.2 \text{ mas yr}^{-1}$, see the left panel of Figure 3). However, for a source with $r = 20.9$ mag, which is close to the *Gaia* limiting magnitude, the combination of PS1, SDSS and *Gaia* can improve the precision of the *Gaia* proper motion by $\Delta\epsilon_\mu \sim 1.0 \text{ mas yr}^{-1}$ (see the right panel of Figure 3).

3. RESULTS AND PERFORMANCE

Using the approach described in Section 2.2 and the method used in GPS1 (see Section 3 of T17), we determine proper motions for around 400 million sources, down to a magnitude of ~ 22.5 in the r-band. Among these sources, about 40% sources are re-measured new proper motions with the Bayesian method described in Section 2.2. The proper motions of the remaining objects are obtained with the previous method used in GPS1. The catalog draws on PS1 Season-AVG and *Gaia* DR2 as the primary data, together with the best available combinations of other surveys. The final catalog uses the robust fit (where all the data points are fitted regardless of outliers), cross-validation fit (where outliers are removed while fitting), and MCMC fit (with which proper motions from *Gaia* DR2 are used as priors while sampling if the proper motions exist in *Gaia* DR2). For reference, we also include the proper motions of *Gaia* DR2 if they exist. Table 1 lists the main columns contained in the catalog. In the following sub-sections, we discuss the precision and accuracy of proper motions in the different cases.

3.1. Proper Motion Uncertainties in the Different Data Set Combinations

The footprint overlap among *Gaia*, PS1, SDSS and 2MASS surveys introduces some complexity: $\sim 14.5\%$ stars are covered by *Gaia*, PS1, and SDSS, $\sim 43.6\%$ by PS1 and *Gaia*, but not SDSS, $\sim 33.9\%$ stars are only observed by PS1, and the remaining 8% by PS1 and SDSS, but not *Gaia*. Therefore, it is necessary to investigate how the final proper motions are affected by combining the different data sets.

Like GPS1, we investigate how the uncertainties in proper motion differ among the following four combinations of data sets: *Gaia* + PS1 + SDSS + 2MASS (GPS), *Gaia* + PS1 + 2MASS (GP), PS1 + SDSS + 2MASS (PD), and only PS1 (PS1). For the catalog table, different surveys are assigned different integer identifiers: 0, 5, 10, and 20 for PS1, 2MASS, SDSS, and *Gaia*, respectively. This defines a *flag* for different survey combinations entering a fit, represented as the sum of the individual survey identifiers. The primary observations are those from PS1, so the positions for each star must include the PS1 detections when fitting for proper motion.

Figure 4 summarizes the distribution of proper motion uncertainties for the four different combinations. The figure is

Table 1
The columns of GPS1+ catalog

	Column	Unit	description
1	obj_id ^a	-	The unique but internal object_id in PS1
2	ra	degree	R.A. at J2015.0 from <i>Gaia</i> DR2
3	dec	degree	Decl. at J2015.0 from <i>Gaia</i> DR2
4	e_ra	mas	Positional uncertainty in right ascension at J2015.0 from <i>Gaia</i> DR2
5	e_dec	mas	Positional uncertainty in declination at J2015.0 from <i>Gaia</i> DR2
6	ra_ps1	degree	Average right ascension at J2010 from PS1 PV3
7	dec_ps1	degree	Average declination at J2010 from PS1 PV3
8	pmra	mas yr ⁻¹	Proper motion with robust fit in $\alpha \cos \delta$
9	pmde	mas yr ⁻¹	Proper motion with robust fit in δ
10	e_pmra	mas yr ⁻¹	Error of the proper motion with robust fit in $\alpha \cos \delta$
11	e_pmde	mas yr ⁻¹	Error of the proper motion with robust fit in δ
12	chi2pmra	-	χ^2_ν from the robust proper motion fit in $\alpha \cos \delta$
13	chi2pmde	-	χ^2_ν from the robust proper motion fit in δ
14	pmra_x	mas yr ⁻¹	Proper motion with cross-validated fit in $\alpha \cos \delta$
15	pmde_x	mas yr ⁻¹	Proper motion with cross-validated fit in δ
16	e_pmra_x	mas yr ⁻¹	Error of the proper motion with cross-validated fit in $\alpha \cos \delta$
17	e_pmde_x	mas yr ⁻¹	Error of the proper motion with cross-validated fit in δ
18	pmra_mcmc	mas yr ⁻¹	Proper motion with MCMC sampling fit in $\alpha \cos \delta$
19	pmde_mcmc	mas yr ⁻¹	Proper motion with MCMC sampling fit in δ
20	e_pmra_mcmc	mas yr ⁻¹	Error of the proper motion with MCMC sampling fit in $\alpha \cos \delta$
21	e_pmde_mcmc	mas yr ⁻¹	Error of the proper motion with MCMC sampling fit in δ
22	pmra_gaia	mas yr ⁻¹	Proper motion from <i>Gaia</i> DR2 in $\alpha \cos \delta$
23	pmde_gaia	mas yr ⁻¹	Proper motion from <i>Gaia</i> DR2 in δ
24	e_pmra_gaia	mas yr ⁻¹	Error of the proper motion from <i>Gaia</i> DR2 in $\alpha \cos \delta$
25	e_pmde_gaia	mas yr ⁻¹	Error of the proper motion from <i>Gaia</i> DR2 in δ
26	n_obsps1	-	The number of SeasonAVG observations used in the proper motion fit
27	n_obs	-	The number of all the observations used in the robust proper motion fit
28	flag ^b	-	An integer number used to flag the different data combination in the proper motion fit.
29	magg	mag	g-band magnitude from PS1
30	magr	mag	r-band magnitude from PS1
31	magi	mag	i-band magnitude from PS1
32	magz	mag	z-band magnitude from PS1
33	magy	mag	y-band magnitude from PS1
34	e_magg	mag	Error in g-band magnitude from PS1
35	e_magr	mag	Error in r-band magnitude from PS1
36	e_magi	mag	Error in i-band magnitude from PS1
37	e_magz	mag	Error in z-band magnitude from PS1
38	e_magy	mag	Error in y-band magnitude from PS1
39	maggaia	mag	G-band magnitude from <i>Gaia</i>
40	e_maggaia	mag	Error in G-band magnitude from <i>Gaia</i>

^a Here obj_id is an internal PS1 ID, which is different from the public ID released in PS1 catalog.

^b In order to label the different survey combinations for proper motion fit, we assign PS1, 2MASS, SDSS, and *Gaia* with different integer identifiers, i.e. 0, 5, 10, and 20, respectively, and define a *flag* with the sum of identifiers of surveys combined.

Table 2
The formal fitting uncertainties of the proper motions in the different data combinations

ID	Mode	19 < m_r < 21		21 < m_r < 22.5		MCMC Sampling ^a	
		$\langle \epsilon_{\mu_{\alpha^*}} \rangle$	$\langle \epsilon_{\mu_{\delta}} \rangle$	$\langle \epsilon_{\mu_{\alpha^*}} \rangle$	$\langle \epsilon_{\mu_{\delta}} \rangle$	$\langle \epsilon_{\mu_{\alpha^*}} \rangle$	$\langle \epsilon_{\mu_{\delta}} \rangle$
		mas yr ⁻¹					
1	GPS (Gaia+PS1+SDSS+2MASS)	2.10±0.64	1.97±0.60	3.18±0.94	2.93±0.82	0.96±0.50	0.85±0.47
2	GP (Gaia+PS1+2MASS)	3.71±2.07	2.98±1.35	5.10±2.34	4.24±1.68	1.03±0.61	0.95±0.58
3	PD (PS1+SDSS+2MASS)	5.12±2.33	4.85±2.22	7.56±3.26	7.16±3.05	-	-
4	PS1 (<i>only</i> PS1)	15.20±9.93	12.75±6.67	21.58±12.67	18.25±9.72	-	-

^a The uncertainties in this column are estimated from the sources with $19.0 < r < 22.5$ mag. In this mode, proper motions are measured with *Gaia* proper motions as priors during MCMC sampling. Therefore, there are no values in the PD and *only* PS1 modes.

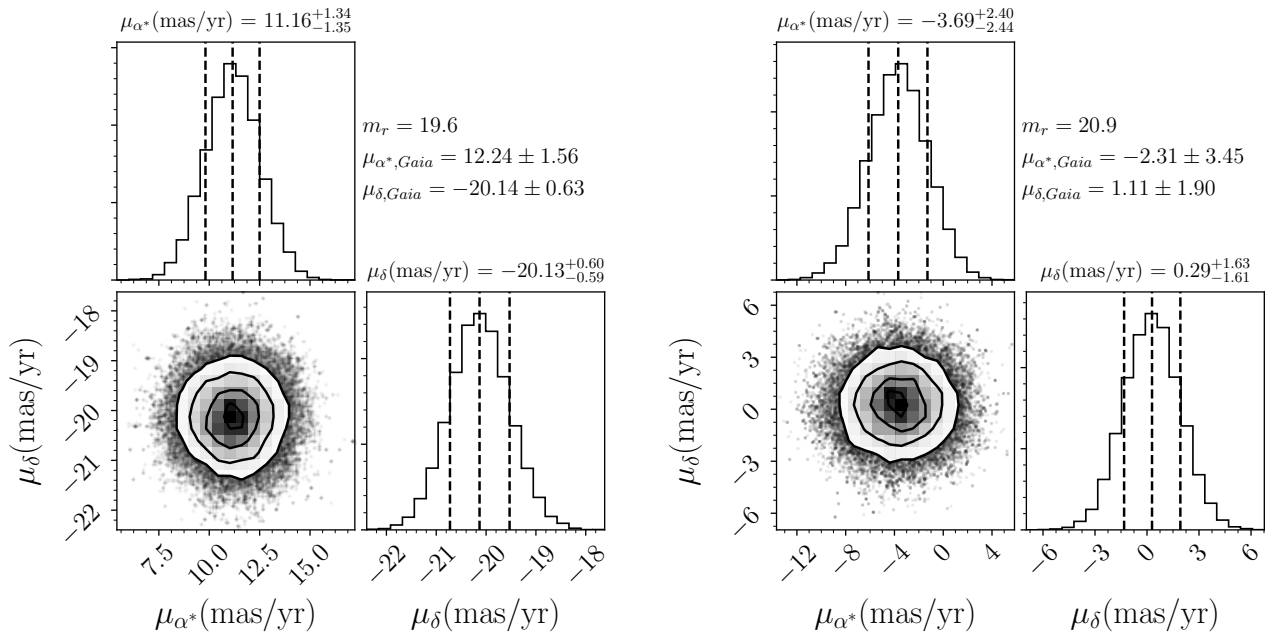


Figure 3. Illustration of the proper motion contours and marginalized probability distributions for two sources with different magnitudes, from the MCMC sampling. The left panel shows the case with a magnitude of $r = 19.6$ mag. In this case, the source is not too faint, the *Gaia* detector works well. Therefore, the proper motions (12.24 ± 1.56 mas yr $^{-1}$ and -20.14 ± 0.63 mas yr $^{-1}$) are well measured in *Gaia* DR2. The precision of new proper motions (11.16 ± 1.34 mas yr $^{-1}$ and -20.13 ± 0.60 mas yr $^{-1}$) can not be improved significantly (only by $\Delta\epsilon_{\mu} \sim 0.2$ mas yr $^{-1}$) via combining the astrometry from SDSS, PS1, and *Gaia*. The right panel displays the case with a magnitude of $r = 20.9$ mag, which is close to the *Gaia* limiting magnitude. In this case, the precision of proper motion can be improved significantly (by $\Delta\epsilon_{\mu} \sim 1.0$ mas yr $^{-1}$) with the combination of the multi-surveys.

drawn with one million sources randomly selected from the GPS1+ catalog. In the four panels, the blue points correspond to the stars in different combinations and the red curves are the median uncertainties in proper motions within different magnitude bins. The average uncertainties in magnitude bins are listed in Table 2, with the mean ($19 < m_r < 22.5$) marked by black lines. In the GPS mode, the average uncertainties are $\epsilon_{\mu_{\alpha^*}} \sim 2.24 \text{ mas yr}^{-1}$ and $\epsilon_{\mu_{\delta}} \sim 2.10 \text{ mas yr}^{-1}$. This is better than the GP mode ($\mu_{\alpha^*} \sim 3.98 \text{ mas yr}^{-1}$ and $\mu_{\delta} \sim 3.19 \text{ mas yr}^{-1}$). SDSS positions improve the precision by $\sim 1.5 \text{ mas yr}^{-1}$ for both the $\epsilon_{\mu_{\alpha^*}}$ and $\epsilon_{\mu_{\delta}}$. Without *Gaia* positions (PD mode), the typical uncertainties become $\epsilon_{\mu_{\alpha^*}} \sim 7.45 \text{ mas yr}^{-1}$ and $\epsilon_{\mu_{\delta}} \sim 7.05 \text{ mas yr}^{-1}$. *Gaia* positions improve the precision by $\sim 4.3 \text{ mas yr}^{-1}$ for both $\epsilon_{\mu_{\alpha^*}}$ and $\epsilon_{\mu_{\delta}}$. For PS1 data alone, the mean uncertainties become $\epsilon_{\mu_{\alpha^*}} \sim 21.03 \text{ mas yr}^{-1}$ and $\epsilon_{\mu_{\delta}} \sim 17.75 \text{ mas yr}^{-1}$. The precision improvement is dominated by *Gaia* and SDSS.

Figure 5 illustrates the distribution of uncertainties of these stars as Mollweide projection maps of the entire 3π region of the sky in equatorial coordinate system, containing one million stars randomly selected. The median uncertainty in each pixel is calculated from hundreds of stars. The median values of the uncertainties are $\sim 8.0 \text{ mas yr}^{-1}$ for μ_{α^*} (the left panel) and $\sim 7.2 \text{ mas yr}^{-1}$ for μ_{δ} (the right panel), as shown in the maps. The uncertainties at high and low declinations are larger, as SDSS data are missing. The small uncertainties in the north Galactic cap are driven by the SDSS observations taken ten or fifteen years ago.

For sources with $19 < r < 21 \text{ mag}$, the GPS1+ catalog is at its best. In this magnitude bin, $\sim 92\%$ sources have *Gaia* positions, and $\sim 79.5\%$ sources have *Gaia* proper motions. Therefore, the proper motions in this bin are dominated by the values obtaining with MCMC fitting. During the fitting, we use *Gaia* proper motions as priors, and combine all the astrometry from *Gaia*, PS1, SDSS and 2MASS. The final uncertainties are better than 1.0 mas yr^{-1} for both $\epsilon_{\mu_{\alpha^*}}$ and $\epsilon_{\mu_{\delta}}$ on average in this bin.

For the fainter sources with $r > 21.0 \text{ mag}$, the positional uncertainties steeply increase with the magnitude. The magnitudes of these sources are beyond *Gaia* or close to PS1 and SDSS limiting magnitudes, so the precision of the obtained proper motions will be worse towards the faint end. As the values in Table 2 show, both SDSS and *Gaia* can improve the precision of the proper motions in the PS1 mode by $\sim 10 \text{ mas yr}^{-1}$ individually, and by $\sim 15 \text{ mas yr}^{-1}$ together. Therefore, *Gaia* and SDSS are comparably important for reducing uncertainties for the faint stars.

We checked the quality of the proper motion fits via the distribution of reduced χ^2 for a random subset of stars. The median values for both μ_{α^*} and μ_{δ} are smaller than 1, implying that most fits are good.

According to the performance, the around 66% sources in the GPS, GP, and PD modes are defined as the primary sources, which have a good precision with an average value of $2.0\text{--}5.0 \text{ mas yr}^{-1}$; while the remaining $\sim 34\%$ sources only have PS1 astrometry, which are defined as the secondary sources with an average precision of worse than 15.0 mas yr^{-1} . The bad precision makes the secondary sources probably have no good applications.

3.2. Proper Motion Validation with QSOs

To validate the derived proper motions, we cross-match the GPS1+ catalog with the QSO candidates from [Hernitschek et al. \(2016\)](#), and randomly select 58,000 QSOs with high

probability in the entire PS1 3π sky region.

Figure 6 displays the histograms of the μ_{α^*} (the top panel) and μ_{δ} (the bottom panel) for the QSOs. The median values of the μ_{α^*} and μ_{δ} are $-0.13 \text{ mas yr}^{-1}$ and $-0.17 \text{ mas yr}^{-1}$, and the dispersions are 4.57 mas yr^{-1} and 5.05 mas yr^{-1} , respectively. The median values suggest that the accuracies of GPS1+ proper motions are better than 0.2 mas yr^{-1} on average for both μ_{α^*} and μ_{δ} . The dispersion values roughly reflect the *rms* of GPS1+ proper motions. Note that the apparent proper motions of QSOs suffer from the impact of differential chromatic refraction (DCR), especially in δ . At high declinations, the δ proper motions are biased by up to 2 mas yr^{-1} . At low declinations, the δ proper motions are under-estimated by $\sim 2.0 \text{ mas yr}^{-1}$. This definitely makes the dispersion values of the QSO proper motions become larger than the true values.

3.3. Comparison with Gaia Proper Motions

Gaia DR2 provides us enough proper motions with good measurements for stars in the entire sky. In GPS1+, we recalculate the proper motions for the sources with *Gaia* DR2 proper motions in two methods: (1) the GPS1 method, in which proper motions are obtained by combining the astrometry of *Gaia*, PS1, SDSS, and 2MASS, regardless of *Gaia* DR2 proper motions; (2) the MCMC method, in which proper motions are obtained by combining the astrometry of *Gaia*, PS1, SDSS, and 2MASS, and using *Gaia* DR2 proper motions as priors during MCMC sampling. For the comparison, we randomly select about half a million of stars which have three kinds of proper motions, simultaneously.

Figure 7 illustrates the comparison of proper motions between our GPS1+ and *Gaia* DR2 for μ_{α^*} (the top sub-panel) and μ_{δ} (the bottom sub-panel). Two typical proper motions are presented: the GP proper motions (the left panel), and the GPS proper motions (the right panel). The median of the differences of proper motions ($\Delta\mu = \mu_{\text{GPS1+}} - \mu_{\text{Gaia}}$) lies within $\pm 0.05 \text{ mas yr}^{-1}$ of zero, implying that the accuracy of GPS1+ proper motion is better than 0.05 mas yr^{-1} for both μ_{α^*} and μ_{δ} . The red bars indicate the average *rms* of GPS1+ proper motion is better than 5.0 mas yr^{-1} in the GP mode, and 3.0 mas yr^{-1} in the GPS mode, respectively. Here, we assume that the proper motions are measured well enough in *Gaia* DR2.

Figure 8 represents the comparison of proper motions between our GPS1+(MCMC) case and *Gaia* DR2 for μ_{α^*} (the left panel) and μ_{δ} (the right panel). The insets are the histograms of the error-weighted difference between the two, e.g. $\hat{\Delta}\mu = (\mu_{\text{ours}} - \mu_{\text{Gaia}}) / \sqrt{\epsilon_{\mu_{\text{ours}}}^2 + \epsilon_{\mu_{\text{Gaia}}}^2}$, where the two ϵ are the errors of our and *Gaia* proper motions. The median of the error-weighted differences (marked by the white dashed lines) for the μ_{α^*} and μ_{δ} are -0.02 ± 0.46 and 0.01 ± 0.52 , respectively. The plot indicates that our proper motions are consistent with *Gaia* at a high level.

3.4. Proper Motions Beyond Gaia

In this section, we explicitly summarize what unique data GPS1+ can offer beyond *Gaia* DR2. Overall, more than 60% sources in GPS1+ are beyond the *Gaia* limiting magnitude. It means that *Gaia* can not reach this part of objects, even in *Gaia*'s next data release. The average precision of proper motions for this part of sources is $\sim 7.0 \text{ mas yr}^{-1}$ if they are measured by SDSS (around one third of them have the astrometry of SDSS). Meanwhile, around 40% sources are measured new proper motions with the Bayesian technique with the goal of improving the precisions of *Gaia* DR2 proper motions at the

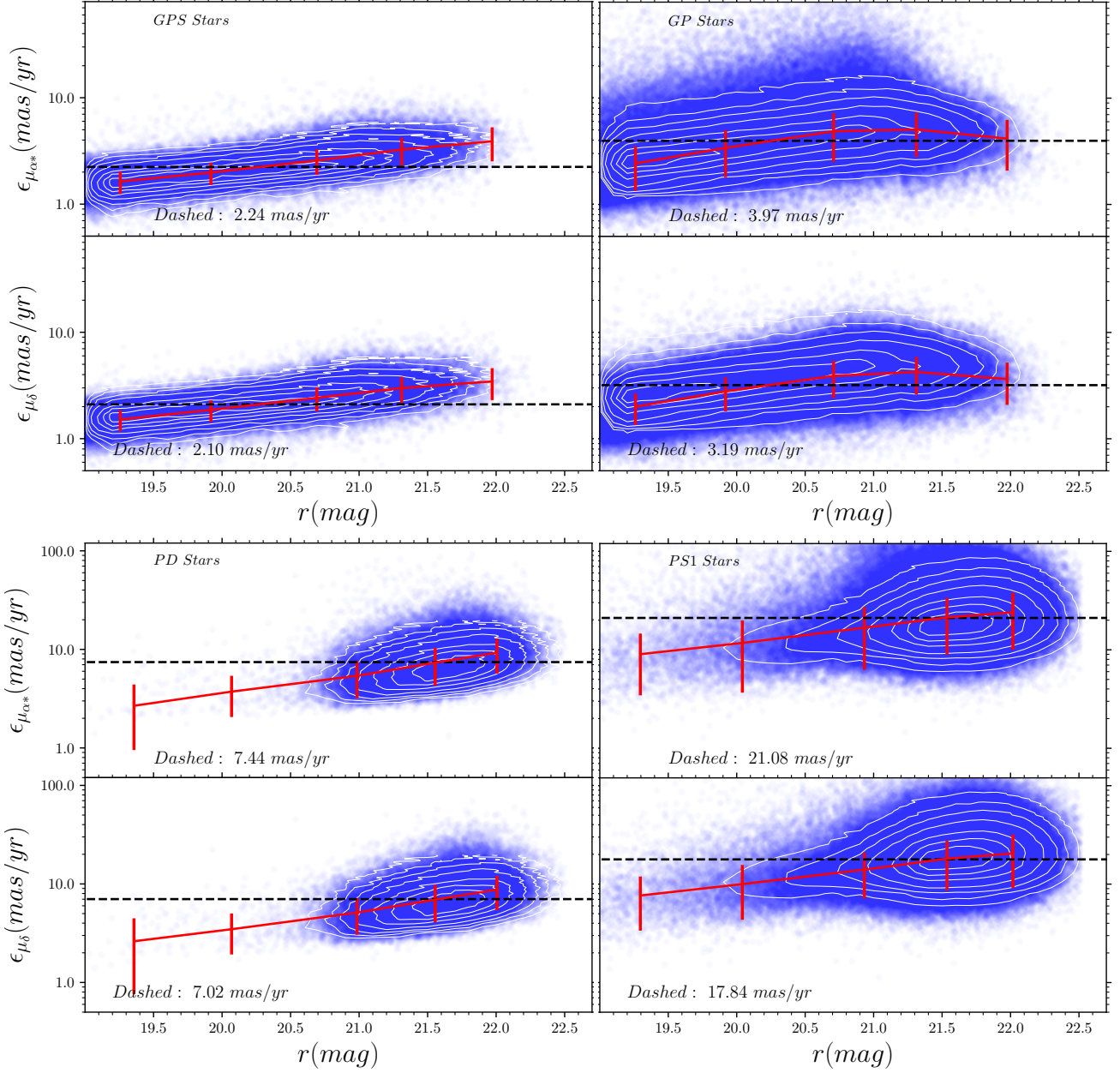


Figure 4. Proper motion precision for the four different combinations of data sets (top-left: GPS, top-right: GP, bottom-left: PD, and bottom-right: ONLY PS1). In the four panels, the red curves and bars are the median uncertainties and *rms* of proper motions within different magnitude bins, and the black dashed lines mark the typical average uncertainties in the magnitude range $19 < r < 22.5$ mag. The blue scatter points represent one million sources randomly selected from the sky. All the uncertainties are logarithmic in every y-axis. The typical average uncertainties for the four combination modes are $\epsilon_{\mu_{\alpha^*}} \sim 2.24 \text{ mas yr}^{-1}$, $\epsilon_{\mu_{\delta}} \sim 2.10 \text{ mas yr}^{-1}$ for the GPS mode, $\epsilon_{\mu_{\alpha^*}} \sim 3.98 \text{ mas yr}^{-1}$, $\epsilon_{\mu_{\delta}} \sim 3.19 \text{ mas yr}^{-1}$ for the GP mode, $\epsilon_{\mu_{\alpha^*}} \sim 7.45 \text{ mas yr}^{-1}$, $\epsilon_{\mu_{\delta}} \sim 7.05 \text{ mas yr}^{-1}$ for the PD mode, and $\epsilon_{\mu_{\alpha^*}} \sim 21.03 \text{ mas yr}^{-1}$, $\epsilon_{\mu_{\delta}} \sim 17.75 \text{ mas yr}^{-1}$ for the ONLY PS1 mode, respectively. The contours indicate the normalized number density of sources with different levels of 0.02, 0.05, 0.1, 0.2, 0.4, 0.6, and 0.8 (the highest density is normalized to 1).

end faint. Moreover, it is worth to mention that around 13% sources are the objects whose proper motions are missing in *Gaia* DR2. We provide the proper motions for these sources in GPS1+ with an average precision $\sim 4.5 \text{ mas yr}^{-1}$.

Figure 9 displays the situations of the proper motions beyond *Gaia* in the different magnitudes. The top panel illustrates the cumulative histograms of the GPS1+ sources ($N_{\text{GPS1+}}$, the black curve), and the sources for which GPS1+ provides proper motions, but *Gaia* DR2 does not ($N_{\text{Gaia,missing}}$, the blue curve), across the 3π sky over the magnitude at the faint region ($r > 19$ mag). The two curves tell us the total $N_{\text{GPS1+}}$ and $N_{\text{Gaia,missing}}$ are about 400 and 47 millions, re-

spectively. The middle panel demonstrates how the ratios of $N_{\text{Gaia},\mu}/N_{\text{GPS1+}}$ (the black curve) and $N_{\text{Gaia,missing}}/N_{\text{Gaia}}$ (the blue curve) vary with magnitudes. Here, $N_{\text{Gaia},\mu}$ and N_{Gaia} are the number of sources for which *Gaia* DR2 provides proper motions in GPS1+, and all the sources for which *Gaia* DR2 provides positions in a magnitude bin, respectively. The black curve suggests that the number of the sources with *Gaia* proper motions drops dramatically at $r > 20$ mag in GPS1+, and there are almost no *Gaia* proper motions beyond $r > 21$ mag. The blue curve demonstrates that the sources whose proper motions are missing in *Gaia* DR2 increase quickly at $r > 20.5$ mag. The bottom panel displays how the

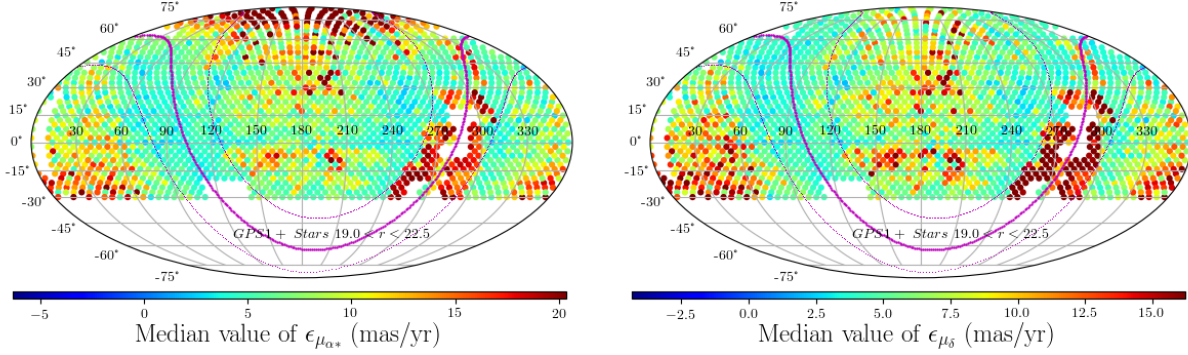


Figure 5. The distribution of proper motion uncertainties for stars with $19 < r < 22.5$ mag; this is illustrated with an equatorial Mollweide projection of the entire 3π sky region. The pink solid ($b = 0^\circ$) and two dotted lines ($b = \pm 20^\circ$) mark the location of the Galactic plane in the equatorial coordinate system, where sources are crowded and the effects of dust extinction are manifest (Tian et al. 2014). To highlight the structures in the maps, the color bar is scaled in $\pm 3\sigma$ around the entire median value for each map.

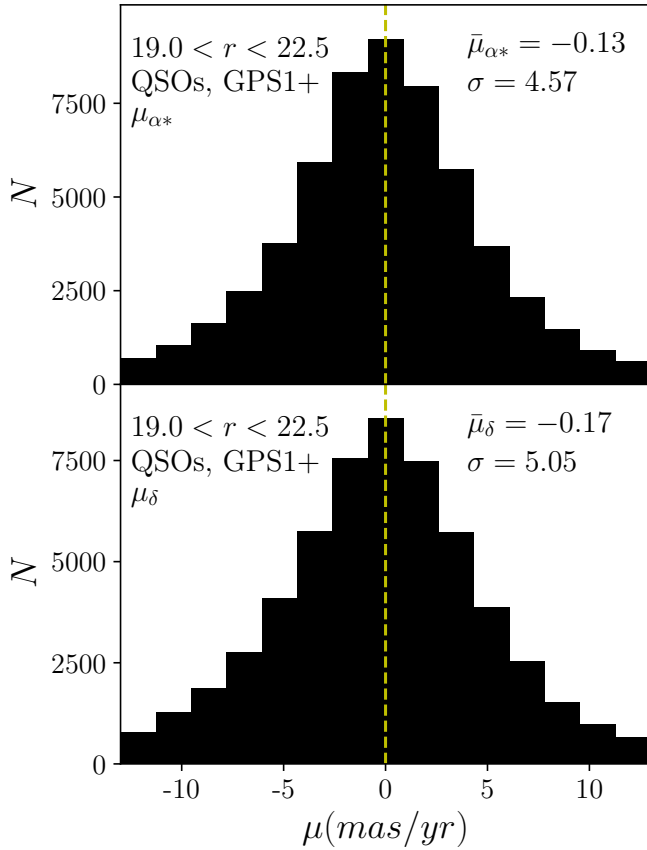


Figure 6. Validation of GPS1+ proper motions with QSOs. The light dashed lines denote zero mas yr^{-1} .

precisions of *Gaia* DR2 proper motions are improved in the different magnitude bins by including PS1 or SDSS astrometry. As the figure shown, the precisions of *Gaia* DR2 proper motions are improved with a limited degree, only by around 0.05 dex at $r < 20.5$ mag. But at $r > 20.5$ mag, the precisions are improved by about 0.1 dex on average.

4. THE VALUES AND LIMITATIONS OF GPS1+

For the most part, GPS1+ constitute a catalog that extends the depth of GPS1 from $r < 20$ mag down to 22.5 mag. It not only fills up some proper motions missed in *Gaia* DR2, but also improves the proper motion precision of faint sources in *Gaia* DR2. The most important point is that GPS1+ pro-

vide new proper motions for a large number of faint sources beyond *Gaia* and other existing catalogs. GPS1+ has important values for the studies involved with faints sources, such as precise age of field stars from white dwarf companions (Fouesneau et al. 2019, Qiu et al. in preparing), brown (Cook et al. 2017; Luhman et al. 2018) or ultracool (Scholz 2020) dwarfs, white dwarf binaries (Parsons et al. 2017; Wang 2018; Gentile Fusillo et al. 2019; Brown et al. 2020; Tian et al. 2020; Wang & Liu 2020), and the sdA problem (Pelisoli et al. 2018a,b, 2019). Moreover, GPS1+ has some potential values for the studies, such as the stellar kinematics (Tian et al. 2017b; Farihi et al. 2018; Wang et al. 2018; Tian et al. 2019), stellar stream (Fu et al. 2018), hypervelocity Stars (Li et al. 2018; Brown et al. 2018), and so on.

In addition, it is worth to summarize the limitations of GPS1+, and where it should be used with caution: (1) Some sources may have erroneous proper motions in crowded regions, e.g., nearby globular clusters, partly because blended sources are easily classified erroneously as extended sources during the reference frame is built, and partly because source crowding may lead to systematic errors in source centering. (2) Some regions are blank in the Galactic plane, particularly in the direction of Galactic center, see Figure 5. So many sources are included in these regions that our pipeline is hard to process these sources. (3) Some sources, e.g., QSOs, are significantly affected by the effect of differential chromatic refraction (DCR). *Gaia* is a space-based telescope, and its observations are not affected by DCR; while PS1 and SDSS are ground-based telescopes and located in different places, so the two surveys suffer from DCR to a different extent. The combination of different surveys in the proper motion fit may lead to complex DCR effects. (4) Around one third of sources in GPS1+, i.e., the so-called secondary sub-sample, have an average precision of worse than 15.0 mas yr^{-1} for their proper motions, because most of them are so faint that they are beyond the capability of *Gaia*'s detector, and only have PS1 astrometry. They may have no good applications due to the bad precision.

5. CONCLUSIONS

Gaia DR2 released proper motions for more than 1.3 billion stars with unprecedented precision in the entire sky region. However, there are some spaces left for the successor of GPS1 proper motion catalog. Firstly, the uncertainties of *Gaia* proper motions increase with magnitudes as a function of power law at the faint region ($r > 19.0$ mag), the

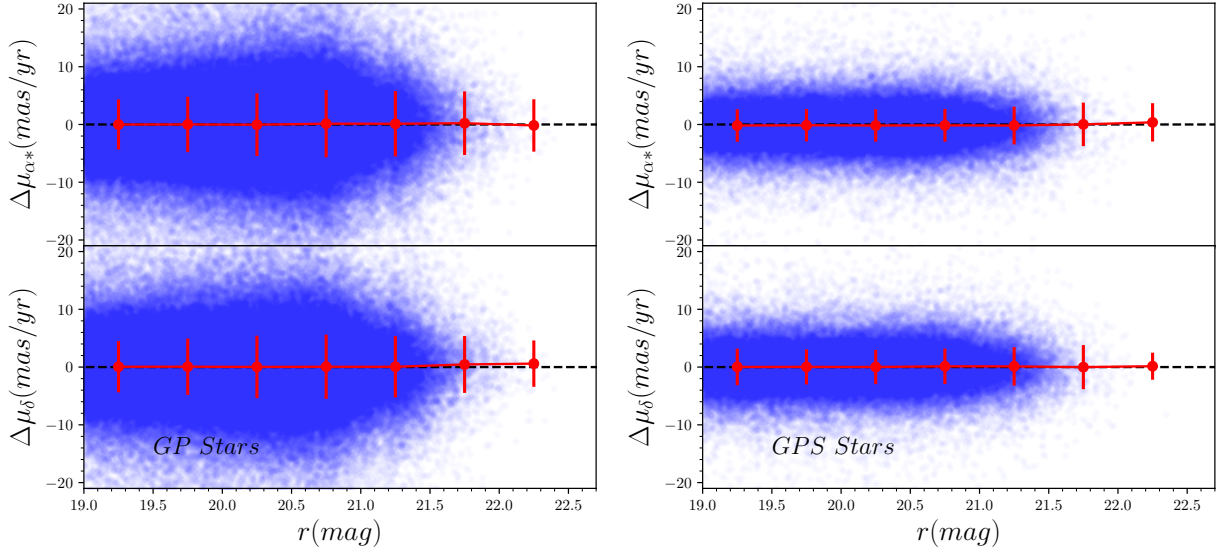


Figure 7. Comparison of proper motions between GPS1+ and *Gaia* DR2 in different magnitude bins. Two typical proper motion modes are presented: the GP proper motions (the left panel), and the GPS proper motions (the right panel). The blue points are the scatters of the differences of proper motions ($\Delta\mu = \mu_{GPS1+} - \mu_{Gaia}$). The red curves are the median values of $\Delta\mu$ in different magnitude bins and the error bars represent the robust *rms*. The black dashed lines mark $\Delta\mu = 0$. All the red points oscillate around the black dashed lines within $\pm 0.05 \text{ mas yr}^{-1}$, indicating that the average accuracy of GPS1+ proper motions is better than 0.05 mas yr^{-1} . The average *rms* in the GP case is $\sim 5.0 \text{ mas yr}^{-1}$, which is reduced to $\sim 3.0 \text{ mas yr}^{-1}$ in the GPS case.

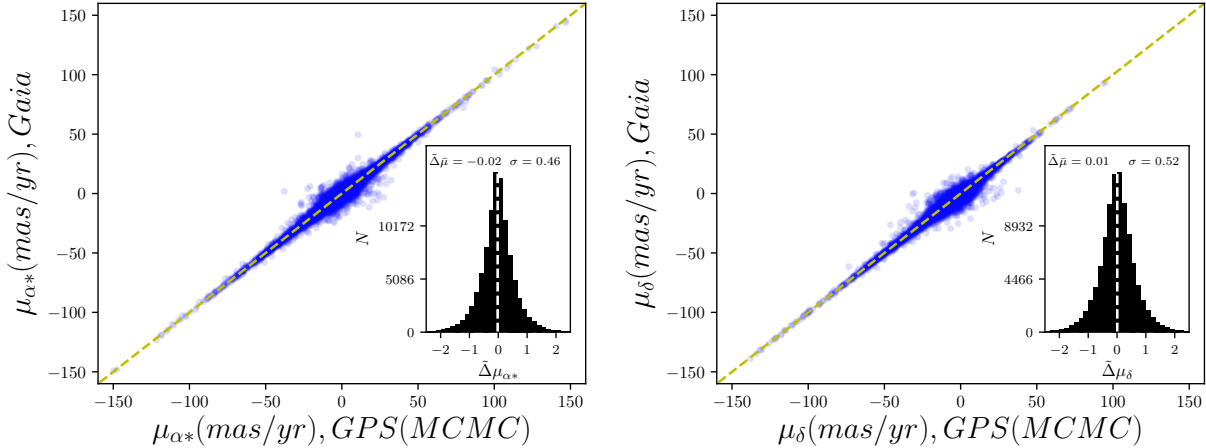


Figure 8. Comparison of proper motions between GPS1+ (MCMC) and *Gaia* DR2 for μ_{α^*} (the left panel) and μ_{δ} (the right panel), based on sources whose proper motions are measured with MCMC fitting. The insets are histograms of the error-weighted difference between our proper motion and *Gaia* DR2. The median of the error-weighted differences (the white dashed line) for the μ_{α^*} and μ_{δ} are -0.02 ± 0.46 and 0.01 ± 0.52 (the absolute values: $-0.03 \pm 0.66 \text{ mas yr}^{-1}$ and $0.01 \pm 0.64 \text{ mas yr}^{-1}$), respectively.

average uncertainty of *Gaia* proper motions become larger than 2 mas yr^{-1} for the sources close to *Gaia* limiting magnitude. Secondly, more than 361 million stars have no proper motions, but have positions in *Gaia* DR2. Thirdly, about 85% PS1 sources have no *Gaia* proper motions in $21 < r < 22.5 \text{ mag}$, which are beyond *Gaia* limiting magnitude. In light of these points, we extend the GPS1 catalog.

With the same procedure of GPS1, we calculated the proper motions for all the PS1 sources fainter than 19 mag in r-band. For the sources with *Gaia* proper motions, we build a Bayesian model by taking *Gaia* proper motions as priors to calculate another new proper motion for each source combining all the available astrometry from *Gaia* DR2, PS1, SDSS, and 2MASS. Finally, we release the GPS1+ proper motion catalog which contains about 400 million point sources down to 22.5 mag in r-band, across three quarters of the sky. The

systematic error (i.e., accuracy) is $< 0.1 \text{ mas yr}^{-1}$, but the typical uncertainty (i.e., precision) in the proper motion of a single source is mode-dependent: $\sim 14.5\%$ sources in the GPS1+ catalog are measured proper motions in the GPS mode, the average precision is $\sim 2.0 \text{ mas yr}^{-1}$, $\sim 43.6\%$ and 8% sources are measured in the GP and PD modes, the precision is $\sim 5 \text{ mas yr}^{-1}$ on average, but $\sim 33.9\%$ sources are only observed by PS1, the typical precision is worse than 15 mas yr^{-1} . Note that $\sim 13\%$ sources are the objects whose proper motions are missing in *Gaia* DR2, GPS1+ provide their proper motion with a precision of $\sim 4.5 \text{ mas yr}^{-1}$, and $\sim 40\%$ sources have *Gaia* proper motions, we re-calculate their proper motions by building a Bayesian model, the final precision of proper motions can be improved up to $\sim 1.0 \text{ mas yr}^{-1}$ relative to *Gaia*'s values at the faint end.

According to the performance, we divide the GPS1+ cata-

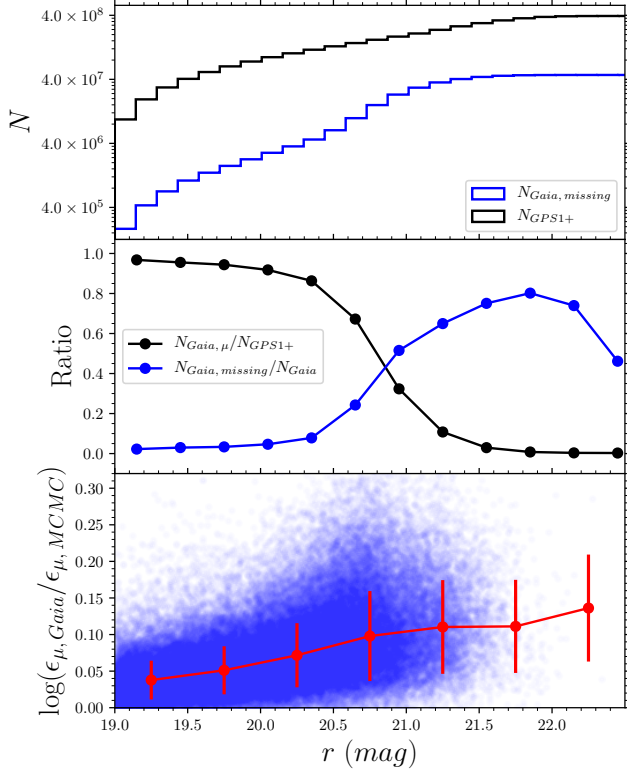


Figure 9. Top: the cumulative histograms of the GPS1+ sources (N_{GPS1+} , the black curve), and the sources for which GPS1+ provides proper motions, but *Gaia* DR2 does not ($N_{Gaia,missing}$, the blue curve) across the 3π sky over the magnitude at the faint region ($r > 19$ mag). Middle: the number ratio v.s. magnitude. The black and blue curves represent the ratios of $N_{Gaia,\mu}/N_{GPS1+}$ and $N_{Gaia,missing}/N_{Gaia}$ in the different magnitude bins, where $N_{Gaia,\mu}$ and N_{Gaia} are the number of sources for which *Gaia* DR2 provides proper motions, and all the sources for which *Gaia* DR2 provides positions in a magnitude bin, respectively. Bottom: the precision improvement factor ($\log(\epsilon_{\mu,Gaia}/\epsilon_{\mu,MCMC})$) of *Gaia* DR2 proper motion at the faint region by the Bayesian technique, where $\epsilon_{\mu,Gaia}$ and $\epsilon_{\mu,MCMC}$ denote the precisions of total proper motions measured in *Gaia* DR2 and with the Bayesian technique in GPS1+, respectively. At $r < 20.5$ mag, the precisions of *Gaia* DR2 proper motions are tiny improved, only by around 0.05 dex. At $r > 20.5$ mag, the precisions are improved by about 0.1 dex on average. Note that this scatter plot is obtained from a sample of one million sources randomly selected from the whole GPS1+ catalog.

log into two sub-samples, i.e., the primary sources with a typical precision of $2.0\text{--}5.0 \text{ mas yr}^{-1}$, which have either or both of *Gaia* and SDSS astrometry; and the secondary sources with an average precision of worse than 15.0 mas yr^{-1} , which only have PS1 astrometry. The bad precision makes the secondary sources probably have no good applications.

The GPS1+ proper motions are validated with QSOs, and the performance is illustrated by comparing with proper motions of *Gaia* DR2.

H.-J.T. acknowledges the National Natural Science Foundation of China (NSFC) under grants 11873034, U1731108, and U1731124. H.-W.R. acknowledges funding from the European Research Council under the European Unions Seventh Framework Programme (FP 7) ERC Grant Agreement n. [321035]. The Pan-STARRS1 Survey (PS1) has been

made possible through contributions of the Institute for Astronomy at the University of Hawaii, Pan-STARRS Project Office, Max-Planck Society and its participating institutes, specifically Max Planck Institute for Astronomy, Heidelberg and Max Planck Institute for Extraterrestrial Physics, Garching, Johns Hopkins University, Durham University, University of Edinburgh, Queen's University Belfast, Harvard-Smithsonian Center for Astrophysics, Las Cumbres Observatory Global Telescope Network Incorporated, National Central University of Taiwan, Space Telescope Science Institute, National Aeronautics and Space Administration under Grant No. NNX08AR22G issued through the Planetary Science Division of the NASA Science Mission Directorate, the National Science Foundation under Grant No. AST-1238877, University of Maryland, Eotvos Lorand University and Los Alamos National Laboratory. This work has made use of data from the European Space Agency (ESA) mission *Gaia* (<https://www.cosmos.esa.int/gaia>), processed by the *Gaia* Data Processing and Analysis Consortium (DPAC, <https://www.cosmos.esa.int/web/gaia/dpac/consortium>). Funding for the DPAC has been provided by national institutions, in particular the institutions participating in the *Gaia* Multilateral Agreement.

REFERENCES

- Altmann, M., Roeser, S., Demleitner, M., et al. 2017, *A&A*, 600, L4
Ahn, C. P., Alexandroff, R., Allende Prieto, C., et al. 2012, *ApJS*, 203, 21
Brown, W. R., Lattanzi, M. G., Kenyon, S. J., et al. 2018, *ApJ*, 866, 39
Brown, W. R., Kilic, M., Kosakowski, A., et al. 2020, *ApJ*, 889, 49
Chambers, K. 2011, American Astronomical Society Meeting Abstracts #218, 113.01
Chambers, K. C., Magnier, E. A., et al. 2016, arXiv:1612.05560
Cook, N. J., Scholz, A., & Jayawardhana, R. 2017, *AJ*, 154, 256
Farihi, J., Arendt, A. R., Machado, H. S., et al. 2018, *MNRAS*, 477, 3801
Fouesneau, M., Rix, H.-W., von Hippel, T., et al. 2019, *ApJ*, 870, 9
Foreman-Mackey, D., Hogg, D. W., Lang, D., & Goodman, J. 2013, *PASP*, 125, 306
Fu, S. W., Simon, J. D., Shetrone, M., et al. 2018, *ApJ*, 866, 42
Gaia Collaboration, Brown, A. G. A., Vallenari, A., et al. 2016, *A&A*, 595, A2
Gaia Collaboration, Brown, A. G. A., Vallenari, A., et al. 2018, *A&A*, 616, A1
Gentile Fusillo, N. P., Tremblay, P.-E., Gänsicke, B. T., et al. 2019, *MNRAS*, 482, 4570
Hernitschek, N., Schlafly, E. F., Sesar, B., et al. 2016, *ApJ*, 817, 73H
Li, Y.-B., Luo, A.-L., Zhao, G., et al. 2018, *AJ*, 156, 87
Luhman, K. L., Herrmann, K. A., Mamajek, E. E., et al. 2018, *AJ*, 156, 76
Parsons, S. G., Hermes, J. J., Marsh, T. R., et al. 2017, *MNRAS*, 471, 976
Pelisoli, I., Kepler, S. O., & Koester, D. 2018, *MNRAS*, 475, 2480
Pelisoli, I., Kepler, S. O., Koester, D., et al. 2018, *MNRAS*, 478, 867
Pelisoli, I., Bell, K. J., Kepler, S. O., et al. 2019, *MNRAS*, 482, 3831
Qi, Z., Yu, Y., Bucciarelli, B., et al. 2015, *AJ*, 150, 137
Roeser, S., Demleitner, M., & Schilbach, E. 2010, *ApJ*, 139, 2447
Scholz, R.-D. 2020, arXiv e-prints, arXiv:2003.10949
Skrutskie, M. F., Cutri, R. M., Stiening, R., et al. 2006, *AJ*, 131, 1163
Stoughton, C., et al. 2002, *AJ*, 123, 485
Tian, H. J., Liu, C., Hu, J. Y., et al. 2014, *A&A*, 561, A142
Tian, H. J., Liu, C., Carlin, J. L., et al. 2015, *ApJ*, 809, 145
Tian, H. J., Gupta, P., Sesar, B., et al. 2017, *ApJS*, 232, 4
Tian, H.-J., Liu, C., Wan, J.-C., et al. 2017, *RAA*, 17, 114
Tian, H.-J., El-Badry, K., Rix, H.-W., et al. 2020, *ApJS*, 246, 4
Tian, H., Liu, C., Xu, Y., et al. 2019, *ApJ*, 871, 184
Wang, B. 2018, *Research in Astronomy and Astrophysics*, 18, 049
Wang, B., & Liu, D. 2020, arXiv e-prints, arXiv:2005.01880
Wang, H., López-Corredoira, M., Carlin, J. L., et al. 2018, *MNRAS*, 477, 2858
York, D. G., Adelman, J., et al. 2000, *AJ*, 120, 1579
Zacharias, N., Finch, C., Girard, T., et al. 2010, *AJ*, 139, 2184
Zacharias, N., Urban, S. E., Zacharias, M. I., et al. 2004, *AJ*, 127, 3043
Zacharias, N., Finch, C., & Frouard, J. 2017, *AJ*, 153, 166